frontiers | Frontiers in Aerospace Engineering

TYPE Original Research
PUBLISHED 14 February 2025
DOI 10.3389/fpace.2025.1454832

OPEN ACCESS

EDITED BY
Zhaodan Kong,
University of California, Davis, United States

REVIEWED BY
John Page,
University of New South Wales, Australia
Krishna Kalyanam,
National Aeronautics and Space Administration, United States

*CORRESPONDENCE
Nicholas Conlon,
nicholas.conlon@colorado.edu

RECEIVED 25 June 2024
ACCEPTED 02 January 2025
PUBLISHED 14 February 2025

CITATION
Conlon N, Acharya A, McGinley J, Slack T, Hirst CA, D'Alonzo M, Hebert MR, Reale C, Frew EW, Russell R and Ahmed NR (2025) Competency self-assessment for a learning-based autonomous aircraft system. *Front. Aerosp. Eng.* 4:1454832. doi: 10.3389/fpace.2025.1454832

Competency self-assessment for a learning-based autonomous aircraft system

Nicholas Conlon[1]*, Aastha Acharya[2], Jamison McGinley[2], Trevor Slack[2], Camron A. Hirst[2], Marissa D'Alonzo[3], Mitchell R. Hebert[3], Christopher Reale[3], Eric W. Frew[2], Rebecca Russell[3] and Nisar R. Ahmed[2]

[1]Department of Computer Science, University of Colorado Boulder, Boulder CO, United States , [2]Department of Aerospace Engineering Sciences, University of Colorado Boulder, Boulder CO, United States, [3]Draper, Cambridge MA, United States

Introduction: Future concepts for airborne autonomy point toward human operators moving out of the cockpit and into supervisory roles. Urban air mobility, airborne package delivery, and military intelligence, surveillance, and reconnaissance (ISR) are all actively exploring such concepts or currently undergoing this transition. Supervisors of these systems will be faced with many challenges, including platforms that operate outside of visual range and the need to decipher complex sensor or telemetry data in order to make informed and safe decisions with respect to the platforms and their mission. A central challenge to this new paradigm of non-co-located mission supervision is developing systems which have explainable and trustworthy autonomy and internal decision-making processes.

Methods: Competency self-assessments are methods that use introspection to quantify and communicate important information pertaining to autonomous system capabilities and limitations to human supervisors. We first discuss a computational framework for competency self-assessment: factorized machine self-confidence (FaMSeC). Within this framework, we then define the generalized outcome assessment (GOA) factor, which quantifies an autonomous system's ability to meet or exceed user-specified mission outcomes. As a relevant example, we develop a competency-aware learning-based autonomous uncrewed aircraft system (UAS) and evaluate it within a multi-target ISR mission.

Results: We present an analysis of the computational cost and performance of GOA-based competency reporting. Our results show that our competency self-assessment method can capture changes in the ability of the UAS to achieve mission critical outcomes, and we discuss how this information can be easily communicated to human partners to inform decision-making.

Discussion: We argue that competency self-assessment can enable AI/ML transparency and provide assurances that calibrate human operators with their autonomous teammate's ability to meet mission goals. This in turn can lead to informed decision-making, appropriate trust in autonomy, and overall improvements to mission performance.

KEYWORDS

machine self-confidence, human-autonomy teaming, intelligent aerospace systems, trustworthy AI, uncrewed aerial vehicles

1 Introduction

Humans stand to benefit greatly from working cooperatively with autonomous systems that can operate in potentially high-risk situations or perform complex and repetitive tasks. However, reliance on robots and autonomous systems should only occur when the human operator is confident that the system can adequately perform the tasks at hand. This willingness to rely is referred to as *trust*, a subjective measure which, in part, is a function of human belief in an agent's *competency*, as well as belief in the predictability and "normality" of the tasking situation (among many other factors) (Israelsen and Ahmed, 2019). In operational contexts, it has been established that the trust developed by a user in an autonomous system may potentially result in an inaccurate understanding of that system's capabilities (Dzindolet et al., 2003). Such misunderstanding raises the potential for the improper tasking of the agent, and subsequent misuse, abuse, or disuse of autonomy in deployment scenarios. One strategy for encouraging appropriate human trust is for an autonomous robot to report its own perspective on tasks at hand (McGuire et al., 2018; McGuire et al., 2019). If done correctly, a user could better judge whether the robot is sufficiently capable of completing a task within desired delegation parameters, thus adjusting user expectations of performance in a manner suitable to the situation at hand. This idea lies at the core of a wide spectrum of algorithmic strategies for generating *soft assurances*, which are collectively aimed at "trust management" (Israelsen and Ahmed, 2019).

Remote information gathering tasks represent an increasingly important use case for autonomous systems, spanning diverse domains such as deep space exploration, scientific data collection, environmental monitoring, agriculture, infrastructure inspection, and security and defense. In this study, we focus on the use case of *intelligence, surveillance, and reconnaissance* (ISR), a term commonly used to characterize missions that employ sensors to gather specifically valuable information. It is often subdivided depending on the intended use of the data gathered by the mission, such as in the defense domain—theater ISR, tactical ISR, and human-portable or small-unit ISR (OASD, 2018). ISR at all levels is becoming increasingly automated and autonomous and is proliferating across domains. Uncrewed aircraft systems (UAS) are being used to surveil battlefields and target locations (Chua, 2012; Cook, 2007), help detect forest fires (Yuan et al., 2015; Sudhakar et al., 2020; Julian and Kochenderfer, 2019), and assess areas after a natural disaster (Ezequiel et al., 2014; Erdelj et al., 2017). In these applications, the human operator is given the role of a supervisor or teammate to one or more ISR platforms.

Of particular interest is small-unit ISR utilizing autonomous UAS. Here, the ISR platforms are generally person-portable and are either launched from a small runway, thrown, or catapulted into the air. They can be fixed- or rotary-wing and are capable of carrying small payloads. They have basic onboard autonomy, which enables path planning and waypoint following. They may also be limited in flight due to size, weight, and power (SWaP) constraints and can be susceptible to inclement weather. Despite some limitations, these platforms can be invaluable in many applications—with little prep time, a small UAS can be deployed to help a fire crew search for the closest fire or help a squad of soldiers safely recon beyond the next hill.

The challenge with small-unit ISR is that, compared to commercial or military pilots (or even pilots of larger platforms like the MQ-1 Predator or MQ-9 Reaper), small UAS operators may receive less training on the operation of their platforms, which could impact trust. For example, soldiers operating the MQ-7 RAVEN require only 10 days of training[1]. Because the operators of these smaller ISR platforms receive less training prior to deployment, they may have limited understanding of the capabilities and characteristics of the aircraft in off-nominal situations (for example, in poor weather conditions). Additionally, these platforms may not possess soft assurances to calibrate trust. Any misunderstanding of capabilities could be amplified by the high stress and workload environments in which soldiers or disaster responders may find themselves, where mis-calibrated trust in a system can be costly, if not mission-ending. A competency-aware autonomous ISR platform could prevent these misunderstandings by calibrating operator trust through outcome assessments and competency reporting.

We here describe an application of the factorized machine self-confidence (FaMSeC) framework, which allows autonomous algorithmic decision-making agents to generate soft assurances in the form of introspective competency reports based on the concept of machine self-confidence (i.e., machine self-trust). We then discuss the generalized outcome assessment (GOA) factor within the FaMSeC framework and how it can be formulated for reinforcing learning-based autonomous small UAS performing simulated ISR missions. As an extension of our previous research (Conlon et al., 2022a), which only considered limited single-target mission scenarios and narrow sets of competencies, we here present a deeper analysis of the performance of GOA for a broader range of mission-relevant competencies as well as its ability to quantify an autonomous aircraft's competencies in a multi-target ISR mission under varying weather conditions featuring a stochastic wind model that must be accounted for in a learned probabilistic world model. We close with a discussion of several challenges in bringing competency-awareness to live platforms and propose directions for future work.

2 Background and related work

This section first reviews reinforcement learning and probabilistic world modeling as a framework for autonomous decision making. It then provides a brief overview of the approach to mission competency assessment for probabilistic decision-making agents. These ideas are developed further in the next section to describe their application for small UAS ISR mission contexts.

2.1 Autonomous decision making and probabilistic world modeling

Probabilistic algorithms for decision-making under uncertainty have been attracting wide attention within the aerospace community

1 https://asc.army.mil/web/portfolio-item/aviation_raven-suas/

(Kochenderfer, 2015). In addition to their deep connections to conventional state-space optimal control and estimation strategies for guidance, navigation, and control (GNC), probabilistic decision-making algorithms based on Markov decision processes (MDPs), partially observable MDPs, and reinforcement learning (RL) offer an attractive and unified framework for enabling autonomy onboard vehicles which must respond to off-nominal events while coping with complex and uncertain dynamics, observations, and model parameters. RL is of particular interest in many autonomous vehicle applications for its ability to simultaneously optimize control/guidance laws and learn complex dynamics models for non-trivial tasks online via repeated experiences (i.e., learning episodes which can incorporate simulated as well as real data). For instance, in relation to the USA ISR domain considered here, much recent research has considered RL-based training of UAS vehicle guidance and control laws to optimize various mission-level objective functions including high-quality information gathering, low-error target tracking, opportunistic communications, and minimum energy consumption (Abedin et al., 2020; Goecks and Valasek, 2019; Jagannath et al., 2021; Mosali et al., 2022; van Wijk et al., 2023)

The objective in RL (Sutton and Barto, 2018) is to select actions that maximize the total reward during a given learning episode. It is formalized as an MDP consisting of the following model components. Let $\mathcal{S} = s_{t=1:\,T}$ be a set of states and $\mathcal{A} = a_{t=1:\,T-1}$ be a set of actions for time indices $t = 1{:}\,T$, where each s_t and a_t is represented as some finite-dimensional vector with continuous and possibly discrete elements. Define $r(s_t, a_t)$ to be the reward function that maps the current state s_t and action a_t to a reward value, and let $p(s_{t+1}|s_t, a_t)$ be the state–action transition dynamics that provide the distribution over the next state s_{t+1} given the current state s_t and action a_t. Finally, let π be a policy that provides an action from any state such that $a_t \sim \pi(s_t)$. An MDP agent seeks the optimal policy to maximize an expected utility function or value function $V(s_t)$ starting from any state, which is defined in terms $r(s_t, a_t)$ and where the expectation is taken with respect to $p(s_{t+1}|s_t, a_t)$ acting under π. Typically, this corresponds to the cumulative expected discounted reward for an infinite horizon or cumulative expected reward under a finite horizon H, starting from state s_t and acting under a given π being given by Equation 1.

$$V^{\pi}(s_t) = \mathbb{E}\left[\sum_{t=1}^{H} r(s_t, a_t)\right]. \tag{1}$$

The methods in RL can be separated into model-free and model-based according to what is being learned by the agent. While model-free methods directly learn the optimal policy π that maximizes $V(s_t)$, model-based RL focuses on learning a model of the environment in which the agent is interacting. Given the demonstrated benefits and flexibility of model-based RL, such as sample efficiency and multi-tasking ability (Ebert et al., 2018; Moerland et al., 2020; Wang et al., 2019), we chose to implement this method rather than its model-free counterpart. As such, this study follows the model-based approach to learn an approximate, probabilistic world model $\hat{p}(s_{t+1}|s_t, a_t)$ of the real environment $p(s_{t+1}|s_t, a_t)$. This model and its predicted states can then be used in conjunction with a planner and a reward function to select the best actions to perform in the real environment. Additionally, as we will show later, the probabilistic world model can be utilized by competency assessment algorithms to predict confidence statistics of the agent's ability to successfully meet mission objectives.

To parameterize the world model $\hat{p}(s_{t+1}|s_t, a_t)$, we use a deep neural network. Since we are predicting the agent's behavior over some time horizon of interest, a recurrent neural network (RNN) that can capture the temporal information is a suitable choice. The training data comes directly from the agent's interaction with the environment, and a random policy is executed to generate a diverse and exploratory trajectory dataset $\mathcal{D} = \{(s_t, a_t, s_{t+1})\}_{t=0:\,T-1}$. The input into the world model is the current state–action pair (s_t, a_t), and the output is a prediction of the next state (s_{t+1}). Then, maximum likelihood is used to optimize the parameters of the network, resulting in a trained world model that is used for planning.

The planning process follows a model predictive control (MPC) paradigm, which allows the agent to plan over some prespecified time horizon while continuously incorporating newly received observations. The MPC also provides the flexibility to use any algorithm, such as a tree-based planner, that can aggregate all the possible actions or a simple random-sampling-based method like random shooting (Nagabandi et al., 2019) to generate action sequences. The focus of this work will be on using a simple random-sampling-based planning algorithm which, while likely to introduce uncertainty into the planning process, alleviates the need to carefully design the planner. This planner is used with the learned world model to predict the future states and generate action sequences. Then, a user-defined, task-specific reward function is used to rank the action sequences from best to worst in maximizing the reward, and typically only the first action from the best action sequence is executed in the real environment, resulting in the next real observation from the environment.

The selection and tuning of the reward function $r(s_t, a_t)$ lies at the core of any RL problem and is especially critical in model-free methods as it comprises part of the optimization criteria. In model-based RL, however, we have the option of either learning the reward function from the environment (Moerland et al., 2020) or designing it independently of the learning process. Among many limitations of directly learning $r(s_t, a_t)$, the biggest is that the real world rarely provides enumerated reward values. In contrast, designing the reward function ourselves makes it amenable to a multitude of tasks and allows the inclusion of factors that can make the agent more safety conscious. Hence, we design a variety of task-specific reward functions that take in a trajectory made via a state–action sequence and output a single value reward.

2.2 Mission competency assessment

The introduction of sophisticated learning-based decision-making autonomy ostensibly yields many benefits for human end-users of small UAS. Well-designed decision-making autonomy can not only significantly enhance overall mission performance by using rigorous data-driven optimization to fully utilize vehicle and sensor platform capabilities but can also alleviate human users of "dull, dirty, and dangerous" tasks that are physically and mentally demanding. For example, UAS pilots and sensor specialists in search-and-rescue missions often need to work

together to remotely pilot a single vehicle while paying attention to data returns from a variety of onboard sensor payloads and also routinely monitor intelligence feeds and other communication channels to adapt mission strategies in dynamic time-critical situations across multiple hours or days (Ray et al., 2024).

Nevertheless, the issue of trust in autonomy has been widely noted as an important barrier to the wider adoption of vehicle autonomy for such applications (Devitt, 2018; Shahrdar et al., 2019). While the topic of trust in human–machine interaction is far too complex to fully discuss here, it is worth noting that the perceived situation normality, predictability, and competency of autonomous systems play a key role in calibrating end-user trust; this in turn has motivated research on a wide range of soft algorithmic assurances for trust calibration and management in user–autonomous system interactions (Israelsen and Ahmed, 2019). Whereas end-users will typically not be technology experts in topics such as vehicle systems, RL, and deep learning, they often will still have valuable domain knowledge that can be usefully leveraged to design soft assurances. Of particular interest here is how soft assurances can be developed to provide a more accurate representation of a learning-based UAS's actual mission capabilities so that end-users can better calibrate their trust in a system and assign tasks that remain within its competency limits.

This study focuses on one particular type of soft assurance for learning-based UAS decision-making autonomy known as *machine self-confidence*. This is defined as an autonomous agent's own perceived degree of competency to execute tasks within desired parameters while accounting for uncertainties in its environment, states, and limited reasoning/execution capabilities (Aitken, 2016; Israelsen, 2019). Note that this definition not only captures "irreducible" uncertainties that naturally arise in particular tasks (i.e., aleatoric uncertainties such as sensor noise) and "reducible" uncertainties that stem from ignorance of model details (i.e., epistemic uncertainties from lack of available data), but importantly, it also considers "meta-uncertainties" related to the agent's ability to process, acquire, and act on (uncertain) information. Thus, machine self-confidence not only assesses the degree to which an agent is uncertain about its own or the environment's state but also the degree to which its models of uncertainty and actions derived from these are suited to the task at hand (Hutchins et al., 2015; Sweet et al., 2016). Colloquially, this may be thought of as an expression of "machine self-trust", akin to the self-trust/self-confidence expressed to a supervisor by a human subordinate who has been delegated with executing particular tasks.

Aitken (2016), Israelsen et al. (2019), and Israelsen (2019) developed the factorized machine self-confidence (FaMSeC) framework to consider the computation of several interrelated (and non-exhaustive/asymmetric) "problem-solving meta-factors" that enable autonomous decision-making agents to generate machine self-confidence assessments in the context of executing tasks described by Markov decision processes (MDPs). For instance, for agents that reason according to policies governed by standard model-based MDPs, three key meta-factors can be quantitatively evaluated relative to user expectations:

1. *Outcome assessment (OA)*: do the sets of possible events, rewards, costs, utilities, etc. for decisions governed by a policy lead to a desirable landscape of outcomes under uncertainty?
2. *Solver quality*: are the approximations used by the system for solving decision-making problems appropriate for the given task and model?
3. *Model validity*: are the agent's learned/assumed models and training data used for decision-making sufficient for operating in the real world?

Computed scores for each factor can be mapped to notional scales with upper/lower bounds, where the lower bound gives a shorthand indication of "complete lack of confidence" (i.e., some aspect of task, environment, or operational context falls completely outside the agent's competency boundaries) and the upper bound indicates "complete confidence" (i.e., all aspects are well within system's competency boundaries). In Israelsen et al. (2019) and Israelsen (2019), a human user study showed that FaMSeC self-confidence computation and reporting improved the ability of human supervisors to assign or reject tasks within/outside the competency boundaries of simulated autonomous vehicles conducting delivery tasks in uncertain adversarial environments. More recent experiments have provided similar findings using the FaMSeC framework with non-learning-based stochastic planning algorithms in both software and hardware simulations of autonomous ground robots performing navigation tasks in uncertain environments (Conlon et al., 2024; Conlon et al., 2022b).

The problem of applying machine self-confidence concepts to learning agents remains open and challenging. The FaMSeC formulation for MDPs naturally extends to a variety of autonomous agents, such as those that must rely on reinforcement learning (RL) to learn optimal policies and behaviors by interacting with uncertain environments. Mellinkoff et al. (2020) considered a simple model-based RL agent, leveraging the FaMSeC outcome assessment metric to modulate exploration/exploitation in sparse reward environments based on degree of confidence in completing tasks. While promising, this approach requires the agent to have well-defined and reasonably small, computationally tractable *a priori* probabilistic models of its task environment and dynamics. This is not feasible for many autonomous learning applications that must rely on more complex black-box models, such as widely used state-of-the-art deep learning neural network models.

In this study, we restrict attention to probabilistic model-based reinforcement learning (MBRL) using deep neural networks. Despite the theoretical connections between MBRL and MDPs, the extension of FaMSeC to deep RL applications is still not entirely obvious or straightforward. Among the most notable issues, current strategies for computing FaMSeC metrics within MDPs assume the availability of (1) tractable, closed-form state transition probability distributions, (2) fixed policy functions or tables, and (3) static well-defined reward functions and utilities.

In RL applications, assumption (1) is invalid for continuous state spaces with complex dynamics or a large number of states, such that state transition densities cannot be expressed in closed form. Assumption (2) is not valid when considering online or constraint-based decision-making strategies, such as model predictive control. Lastly, assumption (3) is invalid since reward functions for RL problems are often highly tuned to achieve desirable behaviors. Arbitrarily rescaling reward values can drastically alter the interpretation and sensitivity of metrics such

as outcome assessment and solver quality, which Aitken (2016) and Israelsen (2019) originally defined via the reward distribution associated with a given policy. In this study, we consider how principles underlying the FaMSeC metrics can be extended to bridge these (and other) gaps.

Self-assessment of an autonomous agent's capabilities for the given task is critical for collaborative efforts with a human supervisor. The self-assessment approach leveraged focuses on *outcome assessment* (OA), one of five FaMSeC factors developed by Aitken (2016), Israelsen (2019), and Israelsen et al. (2019), which seeks to encourage appropriate human trust in an autonomous system. For MDP-based problems, OA describes the confidence that a user-specified margin of success can be achieved based on a set of potential rewards governed by a policy π. Aitken (2016) proposed applying a logistic function to the upper/lower partial moment (UPM/LPM) of the pdf $p(R_\infty)$ for the non-discounted cumulative reward $R_\infty = \sum_{t=0}^{T} R_i$ generated by *a priori* MDP rollouts. The pdf $p(R_\infty)$ in general cannot be represented analytically since it depends on the probabilistic world model, and so instead it is represented empirically using sample rollouts of the policy simulated on the probabilistic world model. Applying the UPM/LPM to the empirical approximation of $p(R_\infty)$ provides a measure of the "expected margin of success" that an agent expects to achieve for completing the MDP task via π over some finite tasking horizon given a minimum total reward threshold R_* defined by the user to reflect their performance expectations,

$$\frac{UPM}{LPM}\Big|_{R_*} = \frac{\int_{R_*}^{\infty}(R_\infty - R_*)\cdot p(R_\infty)dR_\infty}{\int_{-\infty}^{R_*}(R_* - R_\infty)\cdot p(R_\infty)dR_\infty},$$

$$OA = \frac{2}{1+\left(\frac{UPM}{LPM}\Big|_{R_*}\right)^{-1}} - 1 = \frac{UPM - LPM}{UPM + LPM}.$$

This formulation results in OA ∈ [-1,1], which is ultimately mapped into a semantic confidence statement to be provided to the user. Of course, since this formulation depends on MDP rollouts to construct $p(R_\infty)$, many of the implicit assumptions in the previous work are invalid in RL applications, as stated in the previous section: (1) there are no closed-form state-transition probability distributions, and (2) there is no global policy π to follow. As such, MDP rollouts as classically defined are not possible in this framework. However, as discussed in Section 2.1, by leveraging the MPC framework to discern which action to take in combination with the Gazebo environment to facilitate simulated transitions, trajectory rollouts can be simulated to termination from a given configuration of the environment. We can use these simulated trajectories as a surrogate for the MDP rollouts defined in the outcome assessment formulation.

Notwithstanding, there are some notable weaknesses to outcome assessment that can be addressed in this MBRL framework. Cumulative rewards do not contain information relative to the specific or intermediary outcomes of a trajectory. $p(R_\infty)$ is tied to the reward function $r(s_t, a_t)$, of which the elements are not necessarily proportional to user desirability. Additionally, the user-defined margin of success R_*, in terms of reward value, implicitly requires that the user is knowledgeable about the reward function used. More generally, information from a simulated trajectory is summarized entirely as a cumulative reward. Should a user wish to investigate competency relative to more specific outcomes of a complicated task, these are not available. To address these weaknesses, we propose *generalized outcome assessment* (GOA) to provide confidence that a specified margin of success can be achieved based on a set of potential outcomes.

GOA is computed by running N simulation traces for an outcome statistic of interest X with realizations x. These raw outcomes are first broken down into $M > 1$ unranked sets of equivalence classes: $x_1, x_2, \ldots, x_M$. Then, the unranked classes are ranked by order of user desirability and mapping into the domain z: $z_1, z_2, \ldots, z_{M'}$ *ranked* equivalence classes for $M' > 1$ (M' need not equal M in general). An example of raw outcome variables x includes measures such as the number of times the UAS reaches desired waypoints or the specific battery states for the UAV at the end of a mission. Examples of corresponding z variables could include bins for different ranges of the number of waypoints achieved—for example, z_1 = {1-3 waypoints}, z_2 = {3-5 waypoints}, z_3 = {6-8 waypoints}—or integer assignments for battery levels—for example, z_1 = {battery between 0%–10%}, z_2 = {battery between 10%–20%}, etc. In this new z domain, the ranking $z_i > z_j$ implies that outcome z_i is preferable to z_j.

Given a z-domain histogram of simulated outcomes, we next define a minimum expectation of performance relative to z-domain, z_*. The value of z_* is directly related to mission outcomes and, we argue, more interpretable to users compared to the reward-based R_* discussed earlier. In our z-domain battery example above, if a user was interested in the confidence of the UAS being able to complete the mission with at least 10%–20% battery remaining, they would set $z_* = 2$, indicating that bin z_2 = {battery between 10%–20%} is the minimum battery level they would accept to consider the mission a success. The ratio of the upper partial moments to lower partial moments can then be taken relative to z_*:

$$\frac{DUPM}{DLPM}\Big|_{z_*} = \frac{\sum_{z_j \geq z_*}\left(z_j - z_* + 1\right)*P\left(z_j\right)}{\sum_{z_m \leq z_*}(z_* - z_m)*P(z_m)},$$

Next, the value for GOA is computed through a logistic function, such that GOA ∈ $[-1, 1]$:

$$GOA = \frac{2}{1+\left(\frac{DUPM}{DLPM}\Big|_{z_*}\right)^{-1}} - 1 = \frac{DUPM - DLPM}{DUPM + DLPM}.$$

Finally, these GOA values ∈ [-1,1] are mapped into a semantic labelling scheme to be provided to the user. This would assist general users to quickly grasp the competencies of the autonomous system for the given task regardless of the background. A flow diagram of the computation of GOA given the MBRL context is shown in Figure 1. With this approach, we retain the flexibility to characterize competency relative to user defined margins while also allowing for confidence statements relative to any outcome statistic of interest. This formulation is much more generally applicable to complicated tasks undertaken by an autonomous system where self-assessed competency relative to many statistics will be useful to a human operator acting as a supervisor of the system. Particularly for the UAS ISR simulation, we expect that many task outcomes in addition to overall success will play a role in the decision making of the human operator.

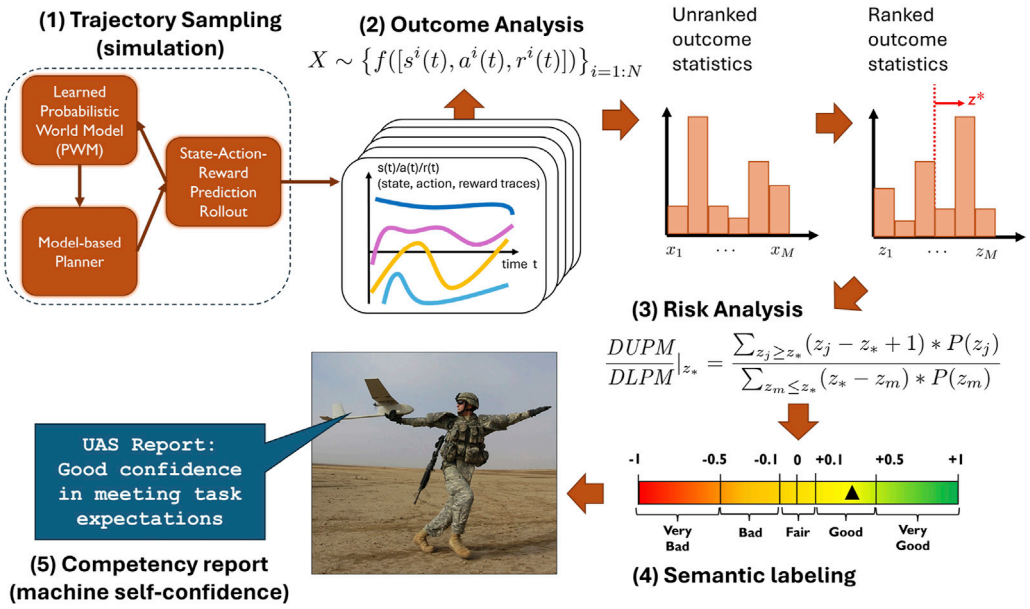

FIGURE 1
Diagram of GOA computation. (1) Simulation traces sampled from a learned world model. (2) Outcome statistics gathered and converted into ranked equivalence classes. (3) DUPM/DLPM statistic is calculated based on $z*$. Finally, the DUMP/DLPM statistic is mapped to a semantic label (4) before being communicated to an operator as a competency report (5).

3 Development of competency assessment in ISR missions

To explore our approach of UAS competency self-assessment for ISR missions, we developed a simulated scenario where a human–UAS team was tasked with surveying several target sites within a broader mission area. The team's collective goal was for the UAS to visit and collect data on as many sites as possible across two missions. The UAS itself is a lightweight, portable, and easily launched platform, similar to the MQ-7 RAVEN. However, due to its small size, it can be adversely impacted by off-nominal environmental conditions, particularly winds at altitude. The first mission's daily weather report predicts calm (nominal) winds, while the second mission's daily forecast is for adverse (off-nominal) winds. Before deploying the UAS, the human supervisor needs to know whether the UAS is capable of achieving their desired outcomes of mission success.

In this section, we discuss the development of a learning-based autonomous UAS capable of self-assessing its mission competencies using GOA. While we note that the MQ-7 RAVEN is capable of flight times in excess of 60 min and operating in a variety of environmental conditions (Pomranky, 2006), we constrain our experiment to a fixed 60 s mission length under both calm and adverse constant wind conditions. This shorter mission duration and limited experimental conditions were chosen to balance model training complexity while still being able to demonstrate GOA analysis of outcome statistics targeted at an ISR platform operating within a realistic mission environment. We believe this contribution to be an important first step in developing methods for future human–UAS teams to utilize competency reports derived from GOA to inform decision-making and improve mission performance in high-risk and uncertain environments.

3.1 Simulation and modeling

Gazebo is a highly customizable, open-source, 3D dynamic multi-robot environment (Koenig and Howard, 2004). It supports a wide variety of platform and sensor models, customized environments, and interfaces with the Robot Operating System (ROS). In addition to modeling the dynamics of our UAS platform, we leverage Gazebo's high-fidelity modeling of terrain, lighting, and various man-made structures to create the realistic mission area for our experiments. Much of our customization took the form of Gazebo plugins, which are shared libraries loaded into Gazebo that enable fine-grained control of most aspects of the simulator. Our plugins modeled the platform's dynamics, its battery, and environmental winds. All communication to and from the plugin was via ROS messaging. Upon start-up, the plugin paused Gazebo and initialized the models with initial UAS state s_0. We followed a *pause–simulate–pause* convention: starting in a paused state, when an action a_t was received, the plugin applied that action to models, unpaused, and simulated Gazebo for k simulation steps, then paused Gazebo and returned the resultant state s_{t+1}. This pattern of *pause–simulate–pause* continued when subsequent actions were received, until the simulation ended.

3.1.1 Platform model

Our platform was modeled as a Techpod fixed-wing UAS from the RotorS package (Furrer et al., 2016). This UAS has a wingspan of 2.6 m, a body length of 1.1 m, and a mass of 2.6 kg. We commanded control surface deflections δ and thrust T by sending a corresponding ROS message to the Gazebo simulator. Control-

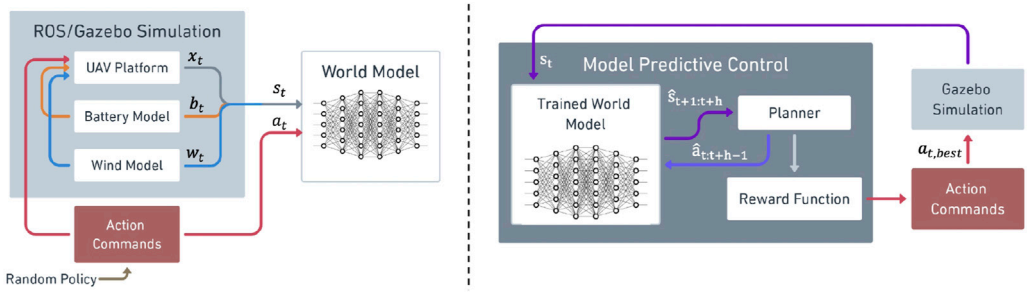

FIGURE 2
Training procedure (left) showing random data being generated and used to train the world model. The planning procedure (right) shows the trained model being used in conjunction with model predictive control to choose optimal actions for the UAS to execute.

surface deflections of the ailerons, elevator, and rudder ranged $\in (-20\text{deg}, +20\text{deg})$, while thrust ranged $\in (0, 1)$, where 0 was no thrust and 1 was maximum. The platform's 6D action space was then $a_t = (\delta_{aileron,t}, \delta_{elevator,t}, \delta_{rudder,t}, T_{x,t}, T_{y,t}, T_{z,t})$.

3.1.2 Battery model

The battery level at time $t+1$, b_{t+1}, followed a simple linear draw model:

$$b_{t+1} = b_t - b_{eff} * T_t * \Delta t$$

—where b_t is the battery level at the previous time step, b_{eff} is a unitless battery efficiency parameter that governs the battery draw rate, T_t is the commanded UAS thrust at time t, and Δt is the duration of the simulation time-step. The battery level estimate at a given time-step was equal to the previous battery level minus the fraction of the battery that was consumed during the previous thrust action. In the event, the battery level reached 0, and our simulation software prevented the platform from executing any further thrust actions. We experimentally tuned the b_{eff} parameter to $b_{eff} = \frac{10}{6}$ so that the UAS had a flight time of approximately 60 s at maximum thrust, aligning with our ISR mission requirements.

3.1.3 Wind model

The wind model simulates the wind disturbances affecting the platform. The model generates wind velocity $w_t = (\dot{w}_{x,t}, \dot{w}_{y,t}, \dot{w}_{z,t})$ at each simulation step. The wind vector is applied uniformly across the entire environment. At each step, the model computes a transformation to the body frame and commands the Gazebo simulator to apply the new wind vector to the platform.

3.1.4 Probabilistic world model

To develop learning-based autonomous UAS, we formulated the problem of predicting UAS state dynamics given previous states, battery information, and wind information through model-based reinforcement learning (Figure 2). The UAS state consists of both translational (x_t, y_t, z_t) and rotational (roll ϕ_t, pitch θ_t, and yaw ψ_t) positions and velocities to fully capture all six degrees of freedom. In addition, we include the wind velocity $(w_{x,t}, w_{y,t}, w_{z,t})$, battery level (b_t), external air temperature (tmp_t), and platform payload mass (p_t) in the state. The complete 18-dimensional state space, including their applicable units and coordinate frames, is shown in Equation 2.

$$\begin{array}{lccc}
\text{Position (meters):} & x_{inertial,t} & y_{inertial,t} & z_{inertial,t} \\
\text{Euler angles (radians):} & \phi_{vehicle-body,t} & \theta_{vehicle-body,t} & \psi_{vehicle-body,t} \\
\text{Velocity (meters/second):} & \dot{x}_{body,t} & \dot{y}_{body,t} & \dot{z}_{body,t} \\
\text{Angular rate (radians/second):} & \dot{\phi}_{vehicle-body,t} & \dot{\theta}_{vehicle-body,t} & \dot{\psi}_{vehicle-body,t} \\
\text{Wind (meters/second):} & \dot{w}_{x,vehicle,t} & \dot{w}_{y,vehicle,t} & \dot{w}_{z,vehicle,t} \\
\text{Battery level (\%):} & b_t & & \\
\text{External air temperature (Kelvin):} & tmp_t & & \\
\text{Payload mass (kilograms):} & p_t & &
\end{array} \tag{2}$$

We model the UAS action space as the instantaneous change in control surfaces and thrust vector. Our six-dimensional action space is shown in Equation 3.

$$\begin{array}{lccc}
\text{Control surfaces (radians):} & \delta_{aileron,t} & \delta_{elevator,t} & \delta_{rudder,t} \\
\text{Thrust (Newton):} & T_{x,t} & T_{y,t} & T_{z,t}
\end{array} \tag{3}$$

One of the main challenges with training neural network world models is ensuring that the input and output data are continuous, normalized, and generalizable to previously unseen data drawn from the training distribution. The absolute positions and Euler angles in the state representation are particularly challenging for these reasons. If using the body frame instead, the gravity vector would have to be explicitly included. We thus formulate the inputs and outputs to the world model in what we call the *model frame* (Figure 3), where gravity is constant. We predict the changes in pose rather than the absolute vehicle pose and then integrate the neural network output. As the coordinate frame changes and integration is fully differentiable, the loss function used for training can still be based on the error in the main state representation. By carefully crafting these data representations for the neural network, we enable the optimization to result in reasonable backpropagated gradients, allowing for stable training and avoiding issues of vanishing or exploding gradients (Bengio et al., 1994; Pascanu et al., 2013).

The pre-processing step for the data input to the RNN world model involves first transforming the vehicle pose and velocity into the model frame and then normalizing the model input representation to have a mean of 0 and standard deviation of 1 over all trajectories.

The post-processing step for the data output from the RNN world model consists of first transforming the change in vehicle pose back into the inertial frame. We then integrate the change in vehicle pose to determine the predicted pose in the inertial frame. Next, we transform the vehicle pose velocity back into the body frame. Finally, we look up the predicted vehicle pose in a wind map to determine the predicted wind vector.

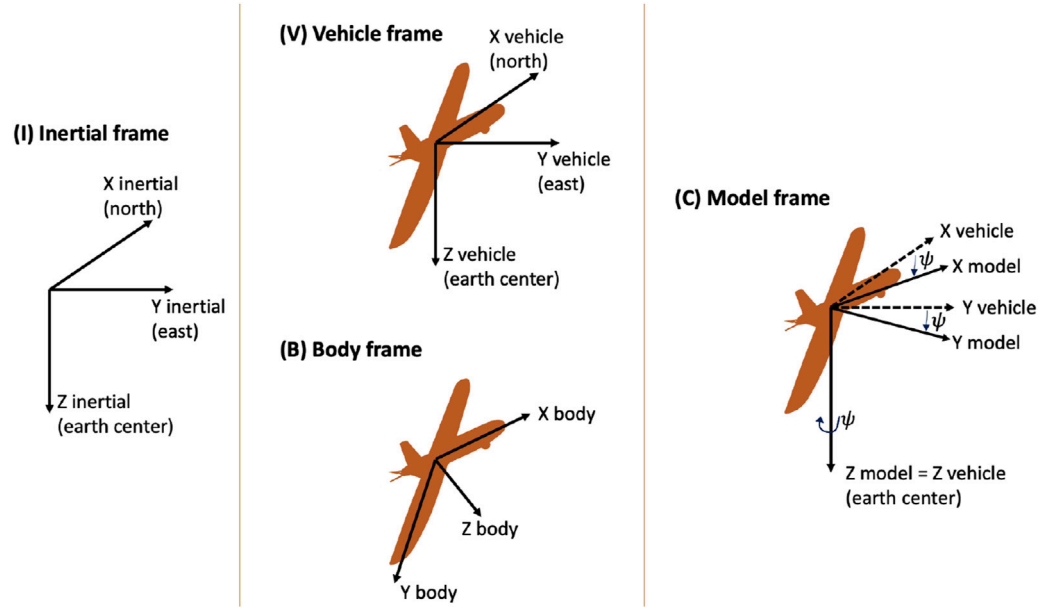

FIGURE 3
Different coordinate frames: (left) inertial frame with origin at Earth's center; (middle, top) vehicle frame with same axes as inertial frame but origin at UAS center of mass; (middle, bottom) body frame with origin at UAS center of mass; (right) model frame, used in our representation, which is an intermediate rotation between vehicle and body frame with rotation only along the yaw axis.

As training data, we first collect 40,000 trajectories by executing random actions in the Gazebo simulation. These trajectories are collected at 1 Hz for a total of 1 min, resulting in 60 length sequences that consist of information on all of the states and actions. Following data collection, we train an RNN that uses a GRU cell to carry through the information from one time step to the next. The model is trained with a depth of 10, meaning that for any given state, the network is asked to predict ten time-steps ahead. The loss then takes on the form shown in Equation 4, where the total loss is the sum of individual losses l_t at each time step. We use mean absolute error as l_t to minimize the error between the predicted output $(\hat{s}_t)$ and the true state (s_t) for a chosen batch size n:

$$loss_{total} = \sum_{t=1}^{10} l_t(s_t, \hat{s}_t), \tag{4}$$

where

$$l_t(s_t, \hat{s}_t) = \frac{\sum_{i=1}^{n} |\hat{s}_{t,i} - s_{t,i}|}{n}$$

is the mean absolute error of the following components of the predicted and true states.

During the planning phase, we use our trained world model in conjunction with the filtering and reward-weighted refinement planner (Nagabandi et al., 2019) to predict a sequence of states given a sequence of actions. Within our MPC setup, the re-planning occurs at every time-step so that only the first action out of the best action sequence as chosen by the reward function is applied to the environment.

3.1.5 Reward modeling

We modeled reward R_t at time step t as the sum of a three-element reward function that can be seen in Equation 5.

$$R_t = R_{targets,t} + R_{safety,t} + R_{battery,t} \tag{5}$$

Each individual reward function R_i uses a tunable parameter x multiplied by an indicator function $\mathbb{1}(\cdot)$, where the target reward

$$R_{target,t} = x_{target} \times \mathbb{1}\left(|UAS_{(x,y,z)} - TGT_{(x,y,z)}| < 25\right),$$

rewards the agent for capturing a target. A target is considered captured if the UAS moves within a 25 m radius of the given target; once a target is captured, it cannot be captured again (i.e., no additional reward is given). The safely reward penalizes the UAS for crashing into the ground plane (altitude = 0) and takes the form

$$R_{safety} = -x_{safety} \times \mathbb{1}(UAS_z <= 0).$$

The battery level reward

$$R_{battery} = x_{battery} \times \mathbb{1}(UAS_{b_t} >= 0),$$

rewards the UAS for conserving the battery life which is expended by the control actions. For our experiments, we tuned our reward parameters to $x_{target} = 10$, $x_{safety} = 0.01$, and $x_{battery} = 0.004$, respectively.

4 Experimental design

We designed two experiments to investigate the ability of generalized outcome assessment (GOA) to evaluate the competency of our autonomous UAS in a time-constrained multi-target visit task under differing wind conditions. Wind speed and its impact on the platform's dynamics is an important factor a user must consider when deciding if and how to deploy a fixed-wing UAS for an ISR mission.

Here, we investigated the ability of GOA to assess the UAS competency across two wind-speed experiments. *Calm* wind represents a nominal operating environment with a constant wind velocity of $w_t = (0, 0, 0)\frac{m}{s}$. *Adverse* wind represents an off-nominal operating environment with a constant wind velocity of $w_t = (5, 5, 0)\frac{m}{s}$. These experiments expand on our previous GOA work analyzing the platform's competency in maintaining a given altitude and maintaining sensor coverage within a single-target zone (Conlon et al., 2022a).

4.1 Multi-target ISR task

We designed a relevant ISR mission where we tasked our autonomous fixed-wing UAS to fly to different target areas within a larger mission area under varying wind conditions. There were six targets available to the platform to visit. Each target had a fixed (x, y, z) location, and all had equal value to the mission. A UAS pass within $25m$ of a target counted as a successful visit, and once a target was visited it did not have to be visited again. We selected set of six targets dispersed throughout the mission area: $Tgt_1 = (-100, 100, 100)$, $Tgt_2 = (100, -100, 150)$, $Tgt_3 = (100, -100, 150)$, $Tgt_4 = (100, 100, 100)$, $Tgt_5 = (200, -200, 150)$, and $Tgt_6 = (200, 200, 100)$.

In each episode, the UAS began at a fixed (x, y, z) location, with initial orientation and velocity selected within a uniform range, $\mathcal{U}(min, max)$. We initialized angle rates to 0. The wind velocity was initialized based the wind condition for each experiment—*Calm* $(w_t = (0, 0, 0)\frac{m}{s})$ or *Adverse* $(w_t = (5, 5, 0)\frac{m}{s})$. The initial battery level was set at 100% and drained with respect to the platform's battery model. Temperature and payload mass were held constant at 288 K and 0 Kg respectively. During the mission, the UAS used the probabilistic world model with model predictive control and the reward function discussed above (3.1.5) to choose the optimal control surface and thrust actions needed to maximize the reward function. This in turn translated into behaviors that visited the targets, conserved battery, and maintained safe altitude. The initial UAS state, s_0, is shown below.

Position (meters):	−300	0	150
Euler angles (radians):	$\mathcal{U}(-\pi, \pi)$	$\mathcal{U}(-0.1, 0.1)$	$\mathcal{U}(-0.1, 0.1)$
Velocity (meters/second):	$\mathcal{U}(0, 30)$	$\mathcal{U}(-5, 5)$	$\mathcal{U}(-2, 2)$
Angular rate (radians/second):	0	0	0
Wind (meters/second):	$w_{x,vehicle,t}$	$w_{y,vehicle,t}$	$w_{z,vehicle,t}$
Battery level (%):	100		
Temperature (Kelvin):	288		
Payload mass (kilograms):	0		

The goal of the task was for the UAS to maximize the number of targets visited (visiting between zero and six targets) while maintaining safe altitude and conserving battery level. We decomposed this high-level goal into three mission outcomes of interest to a potential operator: (1) battery-level conservation, (2) time to the first visit of any of the six targets, and (3) total targets visited of out the six. Given these outcomes of interest, an operator may, before deploying the UAS for this mission, want to know whether the UAS can (1) complete the mission with $X\%$ battery remaining, (2) arrive at the first target within X seconds, and (3) visit X or more targets.

4.2 Competency assessment

To quantify the autonomous UAS's predicted competency in achieving each outcome, we implemented the GOA method covered in Section 2.2. For each experiment (calm or adverse wind), GOA sampled 25 rollouts from the Docker-based Gazebo simulation of the UAS executing the mission. This resulted in a set of 25 60-second trajectory traces that the algorithm then analyzed with respect to each of the three outcomes of interest.

We mapped the raw battery levels to GOA x-domain, $x = [0, 1, \ldots, 100]\%$. The translation to ranked equivalence class, or z-domain, here was trivial, $z = x$. Here increasing z_i equated to a higher battery level at mission completion, which was preferable. The target timing outcome was mapped to the x-domain, $x = [0, 1, \ldots, 60]$ seconds, indicating that the UAS could take 0–60 s to reach the first target. Here, lower time was preferable, so we set z-domain to $z = [60, 59, \ldots, 0]$, such that increasing z_i equated to lower capture time. The x-domain for the total number of targets visited outcome was mapped to $x = [0, 1, \ldots, 6]$ targets. The z-domain, indicating that more targets visited was preferable, was mapped to $z = x$, indicating that more targets visited was preferable. Note that the z-domain could have binned ranges of x; for example, battery level could have used two bins: $z = [(0 - 50\%), (51 - 100\%)]$. However, for simplicity, we chose 1: 1 mapping between the number of elements in the x- and z-domain.

4.3 Hardware resources

All experiments and data analyses were performed on a Dell Precision Laptop running Ubuntu 20.04. The laptop was equipped with an Intel i7 4 core processor, 16 GB RAM, and Nvidia RTX A3000 GPU. All simulation software (code, simulator, and associated scripts) were run within a Docker container. We used the World Model within the Model Predictive Control framework as covered in 3.1.4. For all simulations, we used a 60 s mission time where each simulation step was 1.0 s.

5 Results

We analyzed the generalized outcome assessment (GOA) for both calm and adverse wind conditions. With respect to the algorithm's computational cost, the two main processes underlying GOA are (1) trajectory sampling (simulation) and (2) analysis to include both outcome analysis and risk analysis (Figure 1). Across both experiments, we found that the time taken to sample the set of trajectories was the primary contributor to computational cost $(\mu = 46.7s, \sigma = 0.6s)$ compared to the time taken to analyze the trajectories $(\mu = 0.0005s, \sigma = 0.0005s)$. This is because the time cost of trajectory simulation is based on factors including the complexity of the simulator's dynamics engine, mission time horizon, and mission complexity, while the comparatively fast analysis calculations are only a function of the number of trajectories.

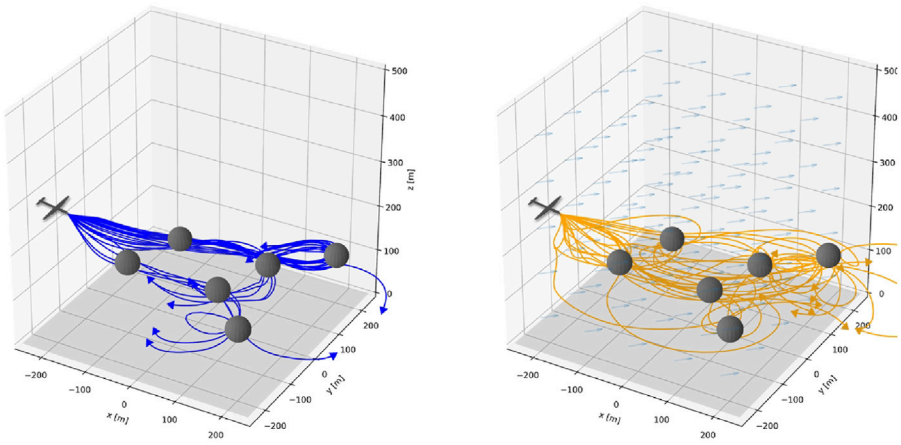

a Calm wind experiment. **b** Adverse wind experiment.

FIGURE 4
Figures of the calm wind experiment (blue trajectories **(A)**) and adverse wind experiment (orange trajectories **(B)**) showing the predicted paths of the UAS as it attempts to capture as many of the six targets (gray orbs) as possible within the mission time limit. UAS silhouette denotes the platform's starting position, while the trajectory arrows show its direction of travel at the end of the task. **(A)** Calm wind experiment. **(B)** Calm wind experiment.

5.1 Wind conditions

Our calm wind experiment simulated wind speeds of $|w_t| = 0\frac{m}{s}$, while our adverse wind experiment simulated wind speed of $|w_t| = 7.07\frac{m}{s}$. Plots of the mission trajectory traces for both experiments can be seen in Figure 4. In the calm wind experiment (Figure 4A), each trajectory followed a relatively smooth and straight path from one target to the next. From the initial state of $(-300, 0, 150)$, the platform's strategy was to either (a) head left to visit the three targets in $+y$, or (b) head right to visit the three targets in $-y$. In the adverse wind experiment (Figure 4B), each trajectory followed a comparatively more random and meandering path due to the off-nominal wind. The platform's strategy is much less obvious here as it is coping with high wind.

5.2 Comparison of outcome distributions and outcome assessments

In this section, we present an analysis of the outcome distributions for each of the three outcomes of interest: *battery level*, *target timing*, and *targets visited*. For each outcome of interest, we discuss the UAS-predicted outcome distributions and how they each translate to the GOA across a range of potential (z_*) values. In all plots, the calm wind experiment is represented in blue, while the adverse wind experiment is represented in orange. GOA tending toward -1 indicates lower confidence in achieving the outcome, while GOA tending toward $+1$ indicates higher confidence. Israelsen (2019) investigated mapping the raw GOA score to semantic labels (e.g., probability words), indicating the machine's self-confidence, where *very bad* $\in (-1.0, -0.5]$ indicates that the GOA algorithm estimated a high certainty that the UAS will fail to achieve the given outcome, *bad* $\in (-0.5, -0.1]$ indicates that the GOA algorithm estimated a high (but not certain) chance the UAS will fail to achieve the outcome, *fair* indicates there is an even chance for failure or success, *good* $\in (0.2, 0.5]$ indicates that GOA estimated a high (but not certain) chance the UAS will achieve the outcome, and *very good* $\in (0.5, 1.0)$ indicates that the GOA algorithm estimated a high certainty that it will achieve the outcome. In this study we analyze the outcome distributions and raw numerical competency self-assessments computed by GOA, but in a real-world human-in-the-loop mission, we foresee these semantic labels being communicated to a user to calibrate them to the platform's competency.

5.2.1 Battery level outcome

Our first outcome of interest is *battery level*. Because a UAS may have to contend with uncertainties in task, environment, weather, and/or potential adversaries, keeping a battery reserve is critical to mission success. An operator may want to know whether the UAS is capable of completing the mission with $X\%$ battery remaining. We measured the battery level as the percentage remaining at the end of the 60 s mission. Figure 5 shows the predicted battery level outcomes for both calm (Figure 5A) and adverse wind conditions (Figure 5B). Looking at both outcome distributions, we can see that the UAS is predicted to be more likely to conserve battery in the calm wind experiment $(\mu = 52\%, \sigma = 23\%)$ than the adverse experiment $(\mu = 27\%, \sigma = 23\%)$. However, there is a large variance in both distributions, indicating a larger uncertainty in the predictions.

Figure 5C shows how these two outcome distributions translate to raw GOA scores. We can see that in both experiments, GOA estimated *very good* confidence $(GOA > 0.5)$ of the UAS being capable of completing the mission with at least 10% or more remaining and estimated *very bad* confidence $(GOA < -0.5)$ of the UAS being capable of completing the mission with 70% or more battery remaining (blue line = orange line). We also see that for ending battery levels between 10% and 70%, GOA estimated that the UAS in the calm wind experiment should have a strictly higher confidence in achieving the battery level outcome compared to the UAS in the adverse experiment (blue line > orange line). This higher

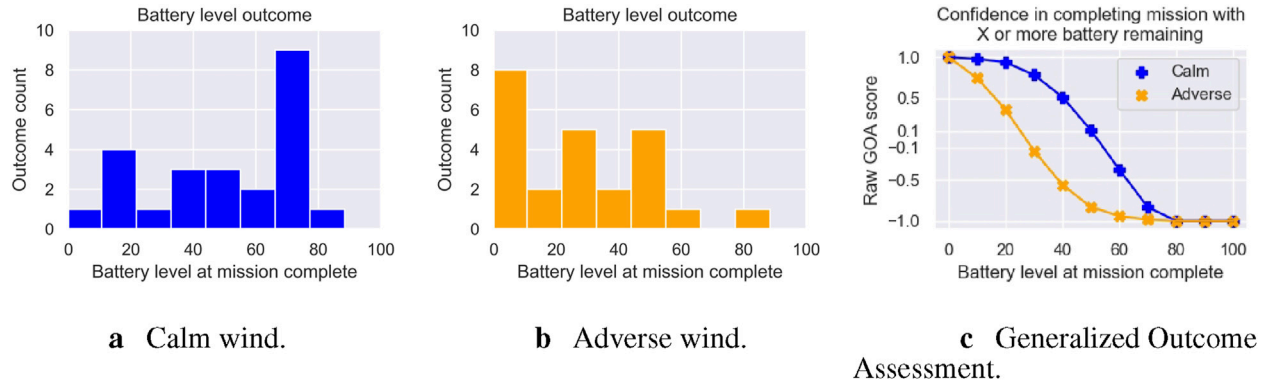

a Calm wind. **b** Adverse wind. **c** Generalized Outcome Assessment.

FIGURE 5
Figures showing battery level outcome distributions across both calm (blue **(A)**) and adverse (orange **(B)**) wind experiments. **(C)** GOA response across all possible ending battery levels, estimating generally higher confidence in the UAS completing the mission with more battery remaining in the calm experiment compared to the adverse experiment. **(A)** Calm wind. **(B)** Adverse wind. **(C)** Generalized outcome assessment.

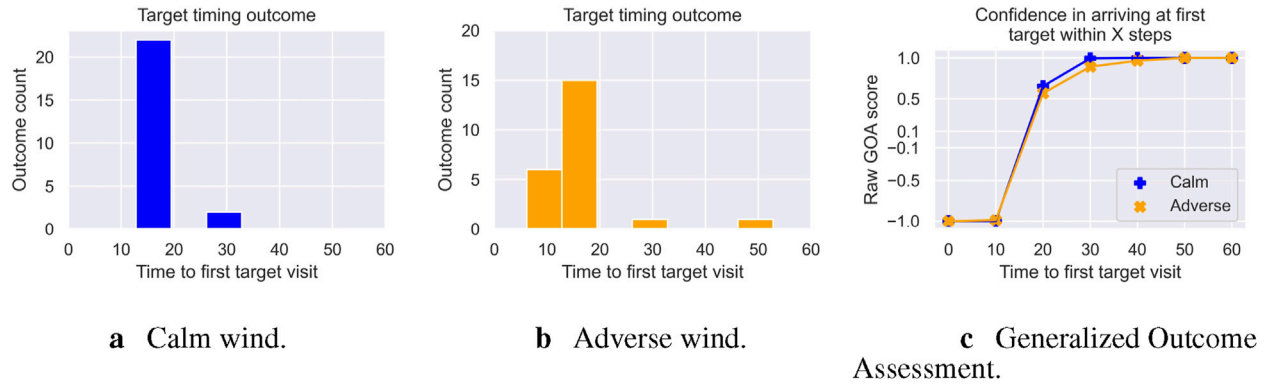

a Calm wind. **b** Adverse wind. **c** Generalized Outcome Assessment.

FIGURE 6
Figures showing the time to first target outcome distributions across both calm (blue **(A)**) and adverse (orange **(B)**) wind experiments. **(C)** GOA response across all possible times to arrive at the first target; UAS has generally higher confidence in visiting the first target faster in the calm experiment than in the adverse experiment. **(A)** Calm wind. **(B)** Adverse wind. **(C)** Generalized outcome assessment.

confidence across the calm wind experiment and lower confidence across the adverse wind experiment is expected, as the UAS would have to expend more thrust and execute more control surface actions in the adverse experiment in order to counteract the higher wind.

5.2.2 Target timing outcome

Our second outcome of interest is *target timing*. For both mission planning and collaborative tasking, it is critical to understand the platform's time on target. We measure time-on-target, or target timing, as the time in seconds for the UAS to visit its first target. Here, an operator may ask whether the UAS is capable of arriving at the first target within X seconds. Figure 6 shows the outcome distributions for both calm (Figure 6A) and adverse (Figure 6B) wind experiments. In the calm wind experiment, the predictions indicate that UAS would visit its first target almost immediately after mission start ($\mu = 17s, \sigma = 4s$). In the adverse experiment, the predictions indicate that the UAS will generally visit the first target quickly ($\mu = 16, \sigma = 8s$) but with a larger variance in the distribution. In some cases, under adverse conditions, the UAS controller may be able to take advantage of the stronger winds and visit the first target faster than in calm conditions, while in others, it may not visit the first target until the last few seconds of the mission time window.

Figure 6C shows the GOA plot for this outcome of interest. We can see both experiments track a similar curve, with the calm experiment showing slightly higher confidence. In both the calm and adverse wind experiments, GOA would estimate *very bad* confidence ($GOA = -1.0$) that the UAS is capable of reaching its first target before $t = 10s$ and estimate *very good* confidence ($GOA = 1.0$) for all times after $t = 20$.

5.2.3 Targets visited outcome

Our third outcome of interest is *total targets visited*. This outcome gives users a sense of how well the UAS will be able to maximize target visits. We measured this as the raw count of targets visited during the 60-s mission. Once a target was visited, it was not counted again. Here, an operator could ask whether the UAS could

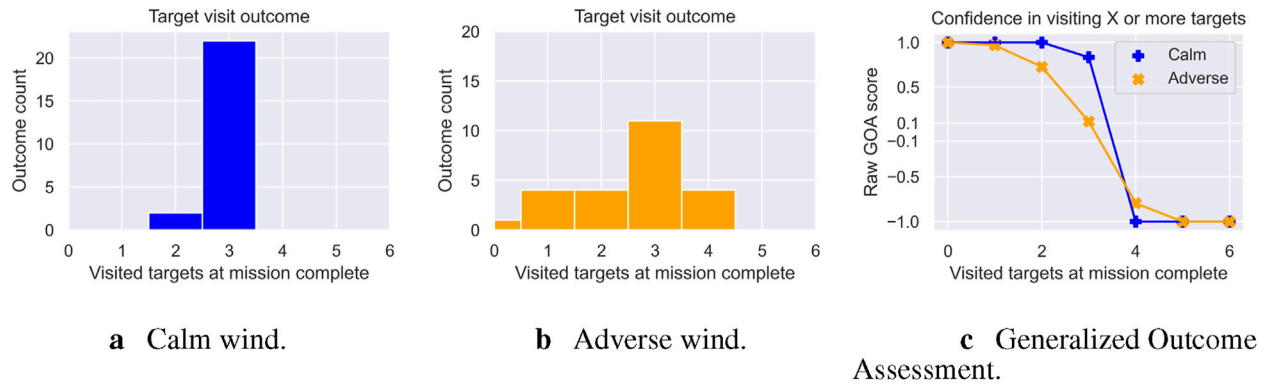

a Calm wind. **b** Adverse wind. **c** Generalized Outcome Assessment.

FIGURE 7
Total targets visited outcome distributions across both calm (blue **(A)**) and adverse (orange **(B)**) wind experiments. **(C)** GOA response across all possible targets, showing that the UAS has generally higher confidence in visiting more targets in the calm experiment than in the adverse experiment. **(A)** Calm wind. **(B)** Adverse wind. **(C)** Generalized outcome assessment.

visit X or more targets within the mission time. Figure 7 shows the outcome distribution for the calm (Figure 7A) and adverse (Figure 7B) wind experiments. As with the target timing outcome, we found a large difference in variance between the two experiments. In the calm experiment, the prediction indicated that the UAS almost always visited three targets ($\mu = 3, \sigma = 0$). While the adverse experiment ($\mu = 2.5, \sigma = 1$) may have a similar mean, the variance captures the mission risk: under adverse conditions, the prediction indicates that the UAS could achieve as many as four or as little as no target visits within the mission time.

This difference in variance impacts the shape of the GOA curve, and in turn, the level of confidence reported to the operator (Figure 7C). Under the calm wind experiment, GOA estimates *very good* confidence ($GOA = 1.0$) that the UAS can achieve up to three target visits during the mission, and *very bad* confidence ($GOA = -1.0$) that the UAS can achieve any more than three. The GOA curve in the adverse wind experiment is shallower, indicating that GOA loses confidence faster in the ability of the UAS to visit targets than in the calm wind experiment (blue line above orange line). However, it is interesting to note that in adverse wind conditions, GOA does show a small amount of confidence that the UAS can visit four of the six targets (orange line above blue line). However, because such an event is quite unlikely, this will be reported as *very bad* confidence.

6 Discussion and future work

Our results indicate that the FaMSeC generalized outcome assessment can be used to assess the competency of an autonomous UAS executing tasks characterized by environmental uncertainty and mission time pressure. We observed that a UAS tasked with operating in calm wind conditions outperformed the same UAS operating in adverse wind conditions across three outcomes of interest to a human supervisor: *battery level*, *target time*, and *targets visited*. The fact that the UAS showed superior performance in the calm wind conditions is expected and obvious. However, given these outcome distributions, we then showed that they can be analyzed using GOA to compute a metric of machine self-confidence in achieving each outcome of interest. We demonstrated that this competency quantification is impacted by both location and the shape of the predicted outcome distributions—GOA captured uncertainties in predicted outcomes that can both add risk and impact performance. We found that the high performance of the UAS during the calm wind experiment led to overall higher GOA confidence in achieving each mission outcome of interest than the UAS during the adverse wind experiment.

As an example of how this may translate to a human–machine team, where the human is supervising the autonomous UAS, consider the human supervisor requesting the following assessments from the UAS in each experiment:

1. "Will the UAS complete the mission with 40% or more battery remaining?" In this case, the calm wind UAS would report back *very good* confidence ($GOA \in (0.5, 1.0)$) in achieving the outcome while the adverse wind UAS would report back *very bad* ($GOA \in (-0.5, -1.0]$). The user can thus easily grasp the wind conditions in which the UAS can successfully maintain battery life.
2. "Will the UAS visit the first target within 20 seconds?" Both the calm wind UAS and the adverse wind UAS would thus report back *very good* confidence ($GOA \in (0.5, 1.0)$). While the platforms may use different strategies due to the wind conditions, both are quite certain in their ability to quickly arrive at the first target.
3. "Will the UAS visit 4 or more targets?" Both the calm and adverse wind UAS would thus report back *very bad* confidence ($GOA \in (-1, -0.5]$), indicating that they are both quite certain each will not achieve such an ambitious outcome. This could lead to a follow up question: "Can the UAS visit 3 or more targets?" Here, in calm winds, the UAS would report back *very good* confidence ($GOA \in (0.5, 1.0)$) while in adverse conditions, the UAS would report back an *even chance* ($GOA \in (-0.2, 0.2]$), giving the user a good indication of the conditions in which the UAS is more capable.

While we are investigating a small set of potential outcomes in a simplistic ISR mission, reported GOA self-assessments should help calibrate human users with their autonomous system's capabilities and lead to improved decision-making with respect to mission execution and platform employment. Previous research has found evidence that communicating competency self-assessments in the ground domain can lead to improvements in user decision-making, with downstream improvements to performance and calibrated trust in the system (Israelsen et al., 2019; Conlon et al., 2022b); however, it is not obvious how such information should be presented to autonomous UAS supervisors, who may be managing far faster and more dynamic platforms. One potential direction for future research is to validate competency self-assessments with GOA in the aerial domain using live platforms with humans in the loop.

Moving toward competency self-assessments for live aerial platforms poses several challenges. The first is the need to quantify and report *in situ* changes to competency. Once a platform is in flight and executing the mission, any *a priori* self-assessments, such as those presented in this work, could be invalidated by changes in the environment (e.g., weather) or the mission (e.g., additional tasking) or the addition of cooperative and non-cooperative platforms (e.g., other aircraft in the area, adversaries). In order to keep human supervisors calibrated to the platform's ability to achieve favorable mission outcomes, the platform should be able to update the assessment as new information becomes available. While such competency updating has been shown to be effective for ground platforms that can safely stop and re-assess (Conlon et al., 2024), the air domain presents a challenge in that fixed-wing platforms that rely on forward motion to generate lift do not have the luxury of temporarily stopping operation while the system and the supervisor decide how to proceed.

This leads to an additional challenge, in that competency self-assessments, particularly those executed *in situ*, need to be computationally fast. We found in this study that the computational bottleneck is in simulating mission rollouts to generate the outcome distributions. We found that this is a function of several parameters, including task time horizon, mission complexity, and the requested number of rollouts. With respect to efficient sampling, research has shown that these distributions can be generated by approximating and intelligently "reusing" rollouts (McGinley, 2022). However, the proposed method has not been directly applied to the aerial domain and may not directly translate to online assessments where previous rollouts can easily be invalidated due to *in situ* changes. Given this, we believe there is ample opportunity to investigate efficient sampling of probabilistic world models, simulations, and digital twins such as those used in this study.

7 Conclusion

As a step toward developing competency-aware decision-making autonomous agents, we developed and analyzed a simulated learning-based autonomous UAS that leverages model-based reinforcement learning to execute a multi-target intelligence surveillance, and reconnaissance (ISR) task. Our UAS used a learned probabilistic world model of its operating environment in conjunction with a stochastic model-based planner to choose optimal actions given a reward function that prioritizes visiting targets, conserving battery, and maintaining a safe altitude. The simulated trajectories capture uncertainties that emerge from both the planner, task, and modeled environment. We showed that we can analyze the trajectories to quantify the system's competency using Factorize Machine Self-Confidence GOA. In particular, we evaluated an autonomous UAS operating in both calm and adverse wind conditions and showed that GOA can capture both performance differences as well as uncertainties across three mission outcomes of interest to potential human supervisors. Additionally, we identified several challenges and directions for future work in translating competency self-assessments to live aerial platforms with humans in the loop. The communication of competency self-assessments to human partners should lead to a safer deployment of the autonomous system and additionally provide UAS operators with the ability to make informed decisions based on the platform's GOA, thus improving the ability to calibrate user trust and understand the system's capabilities.

Data availability statement

The raw data supporting the conclusions of this article will be made available by the authors, without undue reservation.

Author contributions

NC: conceptualization, data curation, formal analysis, investigation, methodology, software, validation, visualization, writing–original draft, and writing–review and editing. AA: conceptualization, formal analysis, investigation, methodology, software, validation, writing–original draft, and writing–review and editing. JM: conceptualization, formal analysis, investigation, methodology, software, validation, writing–original draft, and writing–review and editing. TS: conceptualization, formal analysis, investigation, methodology, software, validation, writing–original draft, and writing–review and editing. CH: conceptualization, formal analysis, investigation, methodology, software, validation, writing–original draft, and writing–review and editing. MD'A: conceptualization, formal analysis, investigation, methodology, software, validation, writing–original draft, and writing–review and editing. MH: conceptualization, formal analysis, investigation, methodology, software, validation, writing–original draft, and writing–review and editing. CR: conceptualization, formal analysis, investigation, methodology, software, validation, writing–original draft, and writing–review and editing. EF: conceptualization, funding acquisition, investigation, supervision, writing–original draft, and writing–review and editing. RR: conceptualization, formal analysis, funding acquisition, investigation, methodology, software, supervision, validation, writing–original draft, and writing–review and editing. NA: conceptualization, funding acquisition, investigation, methodology, supervision, writing–original draft, and writing–review and editing.

Funding

The authors declare that financial support was received for the research, authorship, and/or publication of this article. This work was partially supported by the Defense Advanced Research Projects Agency (DARPA) under Contract No. HR001120C0032.

Acknowledgments

This manuscript represents an extension to our previously presented work (Conlon et al., 2022a).

Conflict of interest

MD'A, MH, CR, and RR were employed by the company Draper.

The remaining authors declare that the research was conducted in the absence of any commercial or financial relationships that could be construed as a potential conflict of interest.

Publisher's note

All claims expressed in this article are solely those of the authors and do not necessarily represent those of their affiliated organizations, or those of the publisher, the editors and the reviewers. Any product that may be evaluated in this article, or claim that may be made by its manufacturer, is not guaranteed or endorsed by the publisher.

Author disclaimer

Any opinions, findings and conclusions or recommendations expressed in this material are those of the author(s) and do not necessarily reflect the views of DARPA.

References

Abedin, S. F., Munir, M. S., Tran, N. H., Han, Z., and Hong, C. S. (2020). Data freshness and energy-efficient uav navigation optimization: a deep reinforcement learning approach. *IEEE Trans. Intelligent Transp. Syst.* 22, 5994–6006. doi:10.1109/tits.2020.3039617

Aitken, M. (2016). *Assured human-autonomy interaction through machine self-confidence*. Boulder: University of Colorado. Master's thesis.

Bengio, Y., Simard, P., and Frasconi, P. (1994). Learning long-term dependencies with gradient descent is difficult. *IEEE Trans. Neural Netw.* 5, 157–166. doi:10.1109/72.279181

Chua, C. N. (2012). *Integration of multiple UAVs for collaborative ISR missions in an urban environment*. Monterey, California, USA: Naval Postgraduate School. Master's thesis.

Conlon, N., Acharya, A., McGinley, J., Slack, T., Hirst, C. A., Hebert, M., et al. (2022a). "Generalizing competency self-assessment for autonomous vehicles using deep reinforcement learning," in AIAA SciTech forum *(AIAA)*.

Conlon, N., Ahmed, N., and Szafir, D. (2024). Event-triggered robot self-assessment to aid in autonomy adjustment. *Front. Robotics AI* 10, 1294533. doi:10.3389/frobt.2023.1294533

Conlon, N., Szafir, D., and Ahmed, N. (2022b). ""I'm confident this will end poorly": robot proficiency self-assessment in human-robot teaming," in 2022 IEEE/RSJ International Conference on Intelligent Robots and Systems (IROS), 2127–2134. doi:10.1109/IROS47612.2022.9981653

Cook, K. L. B. (2007). "The silent force multiplier: the history and role of uavs in warfare," in *2007 IEEE aerospace conference*, 1–7. doi:10.1109/AERO.2007.352737

Devitt, S. (2018). Trustworthiness of autonomous systems. *Found. Trust. Aut. Stud. Syst. Decis. Control* 117, 161–184. doi:10.1007/978-3-319-64816-3_9

Dzindolet, M. T., Peterson, S. A., Pomranky, R. A., Pierce, L. G., and Beck, H. P. (2003). The role of trust in automation reliance. *Int. J. human-computer Stud.* 58, 697–718. doi:10.1016/s1071-5819(03)00038-7

Ebert, F., Finn, C., Dasari, S., Xie, A., Lee, A., and Levine, S. (2018). Visual foresight: model-based deep reinforcement learning for vision-based robotic control. arXiv preprint arXiv:1812.00568

Erdelj, M., Król, M., and Natalizio, E. (2017). Wireless sensor networks and multi-uav systems for natural disaster management. *Comput. Netw.* 124, 72–86. doi:10.1016/j.comnet.2017.05.021

Ezequiel, C. A. F., Cua, M., Libatique, N. C., Tangonan, G. L., Alampay, R., Labuguen, R. T., et al. (2014). "Uav aerial imaging applications for post-disaster assessment, environmental management and infrastructure development," in 2014 International Conference on Unmanned Aircraft Systems (ICUAS), 274–283. doi:10.1109/ICUAS.2014.6842266

Furrer, F., Burri, M., Achtelik, M., and Siegwart, R. (2016). "RotorS—a modular gazebo MAV simulator framework," in *Robot operating system (ROS): the complete reference* (Springer International Publishing), 1, 595–625. chap. RotorS. doi:10.1007/978-3-319-26054-9_23

Goecks, V. G., and Valasek, J. (2019). Deep reinforcement learning on intelligent motion video guidance for unmanned air system ground target tracking. *AIAA Scitech 2019 Forum*, 0137. doi:10.2514/6.2019-0137

Hutchins, A. R., Cummings, M. L., Draper, M., and Hughes, T. (2015). Representing autonomous systems' self-confidence through competency boundaries. *Proc. Hum. Factors Ergonomics Soc. Annu. Meet.* 59, 279–283. doi:10.1177/1541931215591057

Israelsen, B. (2019). *Algorithmic assurances and self-assessment of competency boundaries in autonomous systems*. Boulder: University of Colorado at Boulder. Ph.D. thesis.

Israelsen, B., Ahmed, N., Frew, E., Lawrence, D., and Argrow, B. (2019). "Machine self-confidence in autonomous systems via meta-analysis of decision processes," in *International conference on applied human factors and ergonomics* (Springer), 213–223.

Israelsen, B. W., and Ahmed, N. R. (2019). Dave I can assure you that it's going to be all right a definition, case for, and survey of algorithmic assurances in human-autonomy trust relationships. *ACM Comput. Surv. (CSUR)* 51, 1–37. doi:10.1145/3267338

Jagannath, J., Jagannath, A., Furman, S., and Gwin, T. (2021). Deep learning and reinforcement learning for autonomous unmanned aerial systems: roadmap for theory to deployment. *Deep Learn. Unmanned Syst.*, 25–82. doi:10.1007/978-3-030-77939-9_2

Julian, K. D., and Kochenderfer, M. J. (2019). Distributed wildfire surveillance with autonomous aircraft using deep reinforcement learning. *J. Guid. Control, Dyn.* 42, 1768–1778. doi:10.2514/1.G004106

Kochenderfer, M. J. (2015). *Decision making under uncertainty: theory and application*. MIT Press.

Koenig, N., and Howard, A. (2004). "Design and use paradigms for gazebo, an open-source multi-robot simulator," in 2004 IEEE/RSJ International Conference on Intelligent Robots and Systems (IROS) (IEEE), (Cat. No.04CH37566.

McGinley, J. (2022). *Approaches for the computation of generalized self-confidence statements for autonomous vehicles*. Boulder: University of Colorado. Master's thesis.

McGuire, S., Furlong, P. M., Fong, T., Heckman, C., Szafir, D., Julier, S. J., et al. (2019). Everybody needs somebody sometimes: Validation of adaptive recovery in robotic space operations. *IEEE Robotics Automation Lett.* 4, 1216–1223. doi:10.1109/lra.2019.2894381

McGuire, S., Furlong, P. M., Heckman, C., Julier, S., Szafir, D., and Ahmed, N. (2018). Failure is not an option: policy learning for adaptive recovery in space operations. *IEEE Robotics Automation Lett.* 3, 1639–1646. doi:10.1109/lra.2018.2801468

Mellinkoff, B., Ahmed, N. R., and Burns, J. (2020). "Towards self-confidence-based adaptive learning for lunar exploration," in *AIAA scitech 2020 forum*. doi:10.2514/6.2020-1378

Moerland, T. M., Broekens, J., and Jonker, C. M. (2020). Model-based reinforcement learning: a survey. *arXiv preprint arXiv:2006.16712*

Mosali, N. A., Shamsudin, S. S., Alfandi, O., Omar, R., and Al-Fadhali, N. (2022). Twin delayed deep deterministic policy gradient-based target tracking for unmanned aerial vehicle with achievement rewarding and multistage training. *IEEE Access* 10, 23545–23559. doi:10.1109/access.2022.3154388

Nagabandi, A., Konoglie, K., Levine, S., and Kumar, V. (2019). *Deep dynamics models for learning dexterous manipulation*. arXiv e-prints. arXiv:1909.11652

OASD (2018). "Unmanned systems integrated roadmap 2017-2042," in *Office of the assistant secretary of defense for acquisition Washington United States*.

Pascanu, R., Mikolov, T., and Bengio, Y. (2013). "On the difficulty of training recurrent neural networks," in Proceedings of the 30th International Conference on International Conference on Machine Learning (JMLR.org) (Atlanta, GA, USA: ICML'), III–1310–III–1318.

Pomranky, R. A. (2006). "Human robotics interaction army technology objective raven small unmanned aerial vehicle task analysis and modeling,". Adelphi, MD, USA: US Army Research Laboratory.

Ray, H. M., Laouar, Z., Sunberg, Z., and Ahmed, N. (2024). "Human-centered autonomy for autonomous suas target searching," in *2024 IEEE/RAS international conference on robotics and automation (ICRA 2024)*.

Shahrdar, S., Menezes, L., and Nojoumian, M. (2019). "A survey on trust in autonomous systems," in Intelligent Computing: Proceedings of the 2018 Computing Conference (Springer).

Sudhakar, S., Vijayakumar, V., Sathiya Kumar, C., Priya, V., Ravi, L., and Subramaniyaswamy, V. (2020). Unmanned aerial vehicle (uav) based forest fire detection and monitoring for reducing false alarms in forest-fires. *Comput. Commun.* 149, 1–16. doi:10.1016/j.comcom.2019.10.007

Sutton, R. S., and Barto, A. G. (2018). *Reinforcement learning: an introduction*. second edn. The MIT Press.

Sweet, N., Ahmed, N. R., Kuter, U., and Miller, C. (2016). "Towards self-confidence in autonomous systems," in *AIAA infotech @ aerospace*. doi:10.2514/6.2016-1651

van Wijk, D., Eves, K. J., and Valasek, J. (2023). "Deep reinforcement learning controller for autonomous tracking of evasive ground target," in *AIAA SciTech 2023 forum*, 0128.

Wang, T., Bao, X., Clavera, I., Hoang, J., Wen, Y., Langlois, E., et al. (2019). Benchmarking model-based reinforcement learning. *arXiv preprint arXiv:1907.02057*

Yuan, C., Liu, Z., and Zhang, Y. (2015). "Uav-based forest fire detection and tracking using image processing techniques," in *2015 international conference on unmanned aircraft systems (ICUAS)*, 639–643. doi:10.1109/ICUAS.2015.7152345